Vol. 557: 145–159, 2016
doi: 10.3354/meps11855

MARINE ECOLOGY PROGRESS SERIES
Mar Ecol Prog Ser

Published September 28

Transitions in morphologies, fluid regimes, and feeding mechanisms during development of the medusa *Lychnorhiza lucerna*

Renato M. Nagata[1,2,6,*], André C. Morandini[1,2], Sean P. Colin[3,4], Alvaro E. Migotto[1,2], John H. Costello[3,5]

[1]Departamento de Zoologia, Instituto de Biociências, Universidade de São Paulo, Rua do Matão, trav. 14, n. 101, 05508-090 São Paulo, SP, Brazil

[2]Centro de Biologia Marinha, Instituto de Biociências, Universidade de São Paulo, 11600-970 São Sebastião, SP, Brazil

[3]Marine Biological Laboratories, Woods Hole, MA 02543, USA

[4]Marine Biology and Environmental Science, Roger Williams University, Bristol, RI 02809, USA

[5]Biology Department, Providence College, Providence, RI 02918, USA

[6]*Present address:* Instituto de Oceanografia, Universidade Federal do Rio Grande, Av. Itália, km 8, 96203-000 Rio Grande, RS, Brazil

ABSTRACT: The early ontogeny of scyphomedusae involves morphological and functional transitions in body plans that affect the predators' propulsive and feeding strategies. We applied high-speed videography, digital particle image velocimetry (DPIV), and dye visualization techniques to evaluate alterations in swimming and feeding mechanisms during ontogeny of the rhizostome medusa *Lychnorhiza lucerna* Haeckel, 1880 (Scyphozoa, Rhizostomeae). During early ontogeny, the ephyral mouth lips develop into complex filtering structures along the oral arms. The viscous environments (Reynolds number <100) experienced by ephyrae constrain the feeding mechanisms that transport fluid during ephyral bell pulsations. In contrast, adult medusan fluid flows are dominated by inertial forces, and bell pulsations effectively transport fluids and entrained prey toward the oral arms. The oral arm surfaces are covered by motile epidermal cilia that drive these entrained flows through filtering gaps in the oral arms where food particles are retained. In addition to this process within the oral arms, vortices generated during bell pulsation flow downstream along the outside of the medusae and continuously transport prey toward the exterior oral arm surfaces. Although calanoid copepods are capable of escape velocities that greatly exceed *L. lucerna*'s feeding current speeds, copepods often fail to detect the predator's feeding currents or inadvertently jump into medusan capture surfaces during failed escape attempts. Consequently, the comparatively weak predator feeding currents successfully capture a portion of the copepods encountered by swimming medusae. These results clarify the processes that enable rhizostome medusae to play key roles as consumers in tropical and subtropical coastal environments.

KEY WORDS: Feeding behavior · Foraging mode · Filter-feeding · Jellyfish · Gelatinous zooplankton

INTRODUCTION

Many planktonic predators feed as ambush predators (e.g. hydromedusae and siphonophores), which remain stationary most of the time, waiting for the collision of prey with their expanded capture surfaces (e.g. marginal tentacles) (Costello et al. 2008). In contrast, most scyphozoan medusae (~200 spp.) are filter-feeders that utilize nearly continuous swimming to encounter and capture prey. Periodic bell pulsations of scyphomedusae produce vortices that both generate forward thrust and direct the surrounding fluids downstream (Dabiri et al. 2005). This flux promotes encounter of prey with a predator's

*Corresponding author: renatonagata@gmail.com

feeding structures—the tentacles and the oral arms (Costello & Colin 1994, Dabiri et al. 2005, Acuña et al. 2011).

The utilization of swimming to pump water through feeding structures for prey capture is a widespread mechanism among medusae possessing oblate umbrellas (Costello et al. 2008). Nevertheless, specific prey retention patterns vary due to the diversity of body architectures and prey capture structures (tentacles, oral arms) that trail in the wake behind pulsing scyphomedusan bells. All of these structures are armed with clusters of nematocysts, which discharge and retain prey before they are transported to the mouth opening. The shape and the position of prey capture structures vary widely among scyphomedusan groups. While medusae of Coronatae and Semaeostomeae capture prey with their tentacles and oral arms, species of the derived clade Rhizostomeae (~90 spp.) lack marginal tentacles, and capture prey solely on highly specialized filtering oral arms (Costello & Colin 1995).

The specialized morphology of adult rhizostome medusae contrasts with the simple body plan of the initial medusan developmental stage, the ephyrae, which are very similar among distinct scyphozoan lineages (Russell 1970). The early growth of rhizostome ephyrae involves dramatic size changes that are accompanied by transitions to adult morphologies and feeding strategies. Ephyrae are typically only millimeters in diameter, whereas their adult counterparts usually have larger body size (typically >1 cm bell diameter), with some species attaining bell diameters of 2 m and wet weights of ~200 kg (Kawahara et al. 2006). This means that some species undergo a size transition encompassing 3 orders of magnitude during their planktonic life. Such change imposes functional demands on organisms, since shifts in fluid regimes (i.e. Reynolds number, Re) may alter the functions of body structures (Koehl et al. 2001, Koehl 2004, Higgins et al. 2008, Feitl et al. 2009). These developmental changes in jellyfish dimensions necessitate a transition from fluid environments dominated by viscous forces during ephyral swimming to inertial forces for most adult scyphomedusae.

The feeding strategies by rhizostome medusae have important implications for marine trophodynamics, since these medusae are frequently dominant components of tropical and subtropical marine planktonic ecosystems (Kawahara et al. 2006, Schiariti et al. 2008), with some species (e.g. *Rhizostoma pulmo*) occurring in high densities even in temperate areas (Kramp 1970, Russell 1970). These animals do not merely drift within water masses but are capable of oriented swimming relative to the water currents (Fossette et al. 2015) and complex foraging movements (Hays et al. 2012). Although general aspects of swimming and feeding mechanisms have been described for several rhizostome species (Costello & Colin 1994, D'Ambra et al. 2001, Santhanakrishnan et al. 2012), the exact feeding modes are poorly known in the group, as well as the development of this mechanism during ephyral growth. A mechanical understanding of fluid manipulations by these medusae and the reactions of their prey to these fluid manipulations is important for prediction of resulting planktonic trophic interactions.

Lychnorhiza lucerna Haeckel, 1880 (Scyphozoa, Rhizostomeae) is the most abundant rhizostome in south and southeast Brazil, occurring throughout the year, with seasonal population increases (Morandini 2003, Nogueira 2006). Although these blooms represent a nuisance to shrimp trawlers in Brazil (Nagata et al. 2009) and northern Argentina (Schiariti et al. 2008), information on the trophic role of this medusa species is incomplete. The goals of the present study were (1) to describe sequential morphogenesis of ephyral lips into adults oral arms, (2) to analyze parameters of swimming, bell kinematics, and animal-fluid interaction throughout development, (3) to analyze the fluid motions around swimming medusae and the interaction of wake vortex rings with feeding structures, and (4) to describe predator-prey interaction of *L. lucerna* and calanoid copepods. We focused only on interactions between *L. lucerna* and calanoid copepods since these are the main food items for this species (Nagata 2015). We hypothesized that (1) the development from ephyral to the adult body plans entails a transition in fluid regimes (i.e. Re) that affects both propulsive and feeding strategies, and (2) the sensitivity of calanoid copepods to small hydrodynamic disturbances, coupled with their rapid escape responses, influence predator capture success.

MATERIALS AND METHODS

Sampling and cultivation of medusae

We collected medusae of *Lychnorhiza lucerna* with hand nets in surface waters of Cananéia Estuary (25°04 S, 47°52 W), Southeast Brazil, in March and April 2013. Animals were packed in plastic bags with local seawater and immediately transported to the Centro de Biologia Marinha, Universidade de São

Paulo (CEBIMar-USP) in São Sebastião, São Paulo state, where they were kept inside 5 m^3 containers, with filtered (3 µm) running seawater at ambient temperatures (20–24°C), and fed daily with natural plankton collected with a 200 µm net. Medusae ranged in bell diameter (distance from opposite rhopalia) from 3–7 cm. Ephyrae and young medusae (0.5–3 cm bell diameter) were reared in the laboratory from polyps kindly provided by Dr. Agustin Schiariti (Instituto Nacional de Investigación y Desarrollo Pesquero), from the region of Clamercó, NE coast of Argentina. We maintained polyps following protocols of Jarms et al. (2002) (in the dark, fed weekly, at constant temperature of 22°C, and salinity of 20). Ephyrae were reared in planktonkreisel tanks similar to those described by Raskoff et al. (2003) and fed daily with freshly hatched *Artemia* sp. nauplii.

Ephyral development and formation of filtering oral arms

To describe the serial development of oral arms in *L. lucerna*, we analyzed recently (1 d old) released ephyrae (N = 10) under a stereomicroscope, and photographs were taken with a digital camera (Nikon SMZ1000). Ephyrae were anesthetized with $MgCl_2$ (3.5% in seawater) and photographed daily during the first 20 d, when the animal undergoes a rapid morphological transition, and thereafter, every 5 d, during a total of 2 mo after release. We focused our analyses on morphological development of ephyral manubria into the 8 filtering oral arms of adults. In order to compare the dimensions of capture structures (i.e. digitata) of *L. lucerna* with those of other medusae of Rhizostomeae, digitata length, bulb, stem width, and spacing between consecutive digitata were measured from pictures of live animals.

Video recordings

We placed animals within rectangular aquariums with dimensions of 30 × 40 × 10 cm (width × height × depth) containing filtered seawater. We used 3 imaging set-ups for our analyses: (1) laser sheet illumination for swimming and bell kinematic analyses and for the digital particle image velocimetry (DPIV) quantification of the velocity fields surrounding the animal (e.g. Colin et al. 2013); (2) side-illuminated fluorescein dye visualization of flow for a qualitative description of the interaction between the vortex ring and the inner structures of oral arms; and (3) high-magnification collimated light illumination for predator-prey interactions and prey capture visualization.

The laser sheet was generated using a 530 nm wavelength laser. White light for fluorescein dye and collimated light techniques was generated using light-emitting diodes (LEDs). Videos were recorded at 1000 frames s^{-1} using a high-speed digital video camera (FASTCAM SA3; Photron). Videos for DPIV were recorded with filtered seawater, seeded with hollow glass spheres (10 µm). A laser sheet illuminated a 2-dimensional plane of fluid, and data were collected when the center of the medusa bell was bisected by the laser plane, following Colin et al. (2013). Medusae were left swimming from the bottom to the top of the vessel for at least 3–5 cycles of bell pulsation, and video sequences of a few seconds were recorded. For the fluorescein dye technique, a syringe was used to add the dye near the umbrella margin of swimming medusae. The formation of starting vortex rings and their movements towards the structures of the oral arms were recorded. For videos sequences of predator-prey interactions, medusae were placed swimming around calanoid copepods, which were collected at the São Sebastião Channel, with a 200 µm net. We added only a few copepods inside the aquariums in order to avoid mutual interference between prey during encounters with the medusa. Encounters of *L. lucerna* with copepods of *Acartia* spp. and *Temora turbinata* were recorded at 1000 frames s^{-1}. We analyzed frame-by-frame sequences with copepods with unbroken pairs of first antennae, and escaping responses in a focused plane perpendicular to the camera. The complete escape movement comprised the recoil of the first pair of antennae and the escaping jumps through the reopening of the first antennae.

Data analysis

Bell and swimming kinematics were analyzed using ImageJ software (National Institutes of Health, NIH). All measurements were taken at intervals (t) of 0.01 s for ephyrae and young medusae, and of 0.02 s for larger animals. Alterations in bell shape were measured by the fineness ratio, f, according to Costello & Colin (1994) as:

$$f = H/D \quad (1)$$

where H = bell height, and D = bell diameter.

The contraction angle (c) of the bell margin was measured as the difference between the angle of the bell margin relative to the animal's axis of symmetry

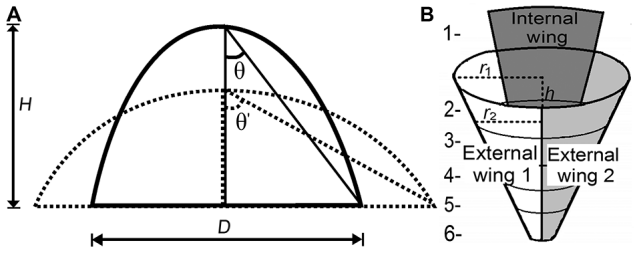

Fig. 1. (A) Measurements of bell kinematics of *Lychnorhiza lucerna*. Dotted line: outline of the bell at the maximum relaxation phase; solid line: outline at maximum contraction. θ′ = bell angle at maximum relaxation; θ = bell angle at maximum contraction, H = bell height, D = bell diameter at maximum contraction. (B) Schematic of the oral arm surface, which comprises 3 wings (2 external and 1 internal). Each wing was subdivided into regions (5 for the external and 6 for the internal wing) according to distance from the bell. r_1 = large radius, r_2 = small radius, h = section height

at the maximum relaxation phase (θ′), and at the maximum contraction phase (θ):

$$c = \theta' - \theta \quad (2)$$

A schematic of the measurements is presented in Fig. 1A.

Distance traveled, m, was measured from sequential changes in position of the anterior-most point of the exumbrellar surface over t intervals. The final and initial position on axes X and Y of the screen were measured using ImageJ software, and the displacement was calculated by applying the Pythagorean theorem:

$$m = \sqrt{(X_f - X_i)^2 + (Y_f - Y_i)^2} \quad (3)$$

where X_f and Y_f are the final and X_i and Y_i the initial position at each axis. Medusa swimming velocity u for a time interval (t) was calculated as:

$$u = m/t \quad (4)$$

Mean swimming velocity u_m was calculated as mean u during 3 successive complete bell contraction cycles.

Reynolds number (Re) was calculated as:

$$\mathrm{Re} = D \times u/v \quad (5)$$

where u is the medusa velocity and v is the kinematic viscosity of seawater at 20°C.

For measurements of flow velocities with DPIV, we used the software package DaVis (Lavision), which analyzes sequential video frames using a cross-correlation algorithm. The frame of reference for all images was the fixed image field through which the animals moved. Velocity fields were integrated over periods of 3–5 frames (3–5 ms), depending on animal size and velocity, in order to allow sufficient particle motion but negligible animal motion during each image pair. Image pairs were analyzed with shifting overlapping interrogation windows of decreasing size (64 × 64 pixels, then 32 × 32 pixels). This analysis generated velocity vector fields around the swimming medusae (Colin et al. 2013). We defined feeding currents as the flows generated by bell pulsations, in the form of vortex rings, which collided with the medusa's prey capture surfaces on their oral arms. We measured the maximum velocities of feeding currents u_f along the full cycle of bell relaxation and contraction by DPIV. Oblate cruising medusae are highly dependent on locally generated flow current to capture prey (Costello & Colin 1994, Dabiri et al. 2005). To achieve a better visualization on how directed flow interacted with oral arms, we calculated fluid velocities along transects at different locations adjacent to the oral arms. At these transects, velocities of fluid motion were decomposed into axial velocities, of a vertical (Y) and a horizontal (X) component. Thus, we could evaluate the importance of fluid transport generated by bell pulsation relative to the position of distal surfaces of prey capture on oral arms. In order to test whether changes in medusae body size were related to changes in biomechanics parameters (e.g. fineness ratio f, contraction angle c, swimming velocity u, Re), the latter were used as dependent variables against bell diameter in linear and non-linear regressions analyses. Before all regression analyses, the assumptions of normality and homogeneity of variances were tested and, when necessary, data were $\log_{10}$-transformed.

Encounters of *L. lucerna* with copepods *Acartia* spp. (N = 38) and *T. turbinata* (N = 40) were characterized for medusae of sizes between 0.6 and 3 cm bell diameter (N = 4). Parameters of encounters were quantified, such as frequency of escape response, prey size (mm), distance from predator where escaping reaction starts (mm), maximum velocity of escape (mm s^{-1}), distance traveled during escapes (mm), turning angles before escape (degrees, °), escape angles relative to predators feeding structures (°), and duration of escapes (s).

Prey capture maps

In order to generate a map of prey captures on the oral arms, we quantified prey captures along the surface of oral arms of medusae (n = 5). Animals were incubated in a container with filtered (3 µm) sea-

water and *Artemia* spp. nauplii for 2 min. After incubation, individuals were carefully removed and preserved in a 4% formaldehyde solution in seawater. We quantified the number of nauplii in 4 oral arms (of a total of 8 oral arms) of each individual under a stereomicroscope. The oral arm surface is comprised of 3 wings (2 external and 1 internal), and each wing was subdivided into regions (5 for the external and 6 for the internal wing) according to the distance from the bell (Fig. 1B). In order to estimate prey capture per unit area (cm^2), we estimated the oral arm surface area as the surface of a truncated cone:

$$Sob = \pi(r_1 + r_2)\sqrt{h^2 + (r_1 - r_2)^2} \quad (6)$$

where r_1 = large radius, r_2 = small radius, and h = section height, according to Fig. 1B. ANOVA analyses were applied to test differences in captures between the 3 oral wings and between regions on each oral wing. Normal distribution (Shapiro-Wilk's W test) and homogeneity of variances (Bartlett test) were tested before these analyses and Kruskal-Wallis tests were used if necessary.

RESULTS

Morphological transition and development of filtering oral arms

Recently released *Lychnorhiza lucerna* ephyrae (3–5 mm bell diameter) typically have a flat bell, a margin with gaps between the 8 lappets, and a cross-shaped central mouth (Fig. 2A). Three to 5 d after release, the margin of the mouth developed many finger-like projections, armed with terminal nematocyst clusters, called digitata (Fig. 2B). As bell diameter reached 12 mm, gaps between adjacent lappets were filled and bell margins became continuous. In 12–20 d old ephyrae (8–20 mm), the tips of the cross-shaped mouth branched to the 8 oral arms (Fig. 2C). In 20–30 d old ephyrae (10–25 mm), as oral arms developed radially, many lateral folds arose along their surfaces (Fig. 2D). These folds developed laterally to cover spaces between adjacent oral arms (Fig. 2D). Still, the distal region of oral arms branched further and gave rise to the 2 external wings (*E1* and *E2*, Fig. 2E) and the central mouth aperture was obliterated. The oral arm transitioned to a filtering surface, and the branching pattern of oral arm edges then contained many gaps of circular-polygonal shape, which structurally resembled a sieve (Fig. 2F). Two months after release (~2 cm bell diameter) and throughout further development, the oral arms elongated distally and became increasingly cone-shaped (Fig. 2G). The oral arms possessed a complex 3-dimensional structure, with a highly ramified edge that operated as a continuous suctorial surface (Fig. 2H). Captured prey were transferred to the oral arm canal system through many millimeter-width pores of the canal inlets (Fig. 2H).

Ontogenetic changes in bell kinematics and pulsation mode

The bell outline had differences in both contraction and relaxation phases between ephyrae and adult animals (Fig. 3). A larger portion of the ephyrae bell (from the bell margin to near the bell apex) moved during both contraction and expansion (Fig. 3A,C). In ephyrae, the expansion movement led to a partial inversion of the bell (Fig. 3A). In adults, only the distal portion close to the bell margin moved, whereas the region representing ~50% of the bell center to bell margin distance remained largely immobile (Fig. 3B,D). The contraction of the bell in ephyrae is 2× faster than the relaxation, and 4× faster than the bell contraction of adults (Fig. 3).

The fineness ratio (f) and bell contraction angle (c) throughout the bell pulsation cycle also changed along the transition from ephyra to adult stages (Fig. 4). For ephyrae, the average f was lower (f = 0.2–0.5) and increased up to dimensions larger than ~2 cm of bell diameter, when f reached a relatively stable adult bell shape (f = 0.5–0.8) (Fig. 4A). Similarly to f, c also changed during early development with wider movements of contraction and expansion in ephyrae (c = 48–78°), whereas c decreased and reached a relatively constant level at diameters above ~2 cm (c = 28–35°) (Fig. 4B).

L. lucerna undergoes a transition in its fluid environment (as Reynolds number, Re) during growth. In ephyrae with diameters <1.5 cm ($\log_{10}$ bell diameter <1.17), maximum Re was <325 ($\log_{10}$ Re < 2.5) and predominantly near 50 ($\log_{10}$ Re ~1.7) (Fig. 5A). For Re in the range of 1 < Re < 100, where ephyra swimming predominantly occurred, both viscous and inertial forces were important. In contrast, the fluid environments of larger medusae, diameters >2.5 cm ($\log_{10}$ bell diameter >2.4), were characterized by higher mean and maximum Re of >300 and >800, respectively ($\log_{10}$ Re >2.5 and >2.9). In this range, fluid environments were dominated by inertial forces (Fig. 5).

In order to understand the effect of body size on swimming kinematics and on the strength of feeding

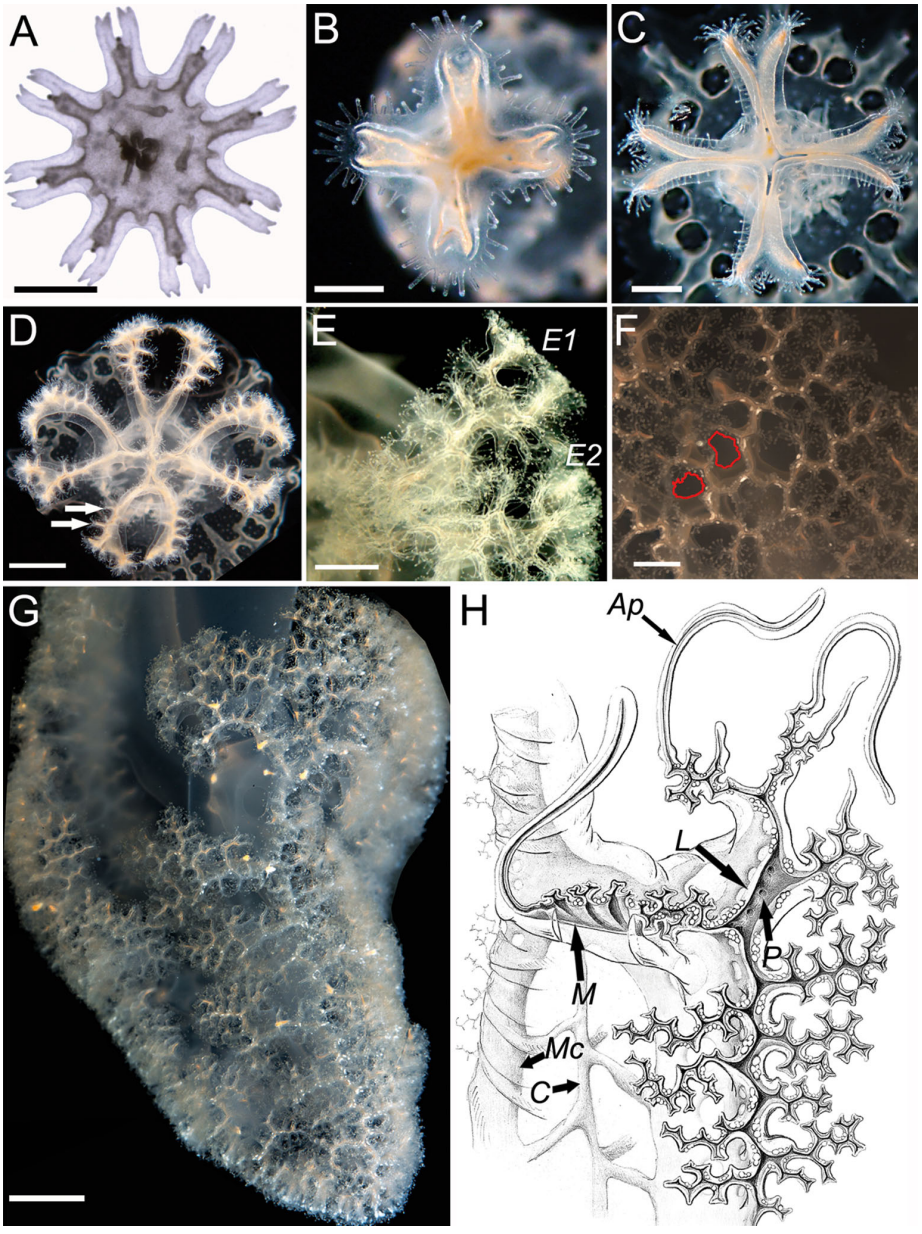

Fig. 2. *Lychnorhiza lucerna*. (A) 1 d old ephyra with a cross-shaped mouth without digitata. (B) Mouth of a 5 d old ephyra with digitata along edges. (C) Mouth of a 14 d old ephyra with the oral lips distally divided to 8 perradial oral arms. (D) 20 d old ephyra; oral arms developed radially, with many lateral folds (arrows), and opening of the central mouth still remains. (E) Tips of oral arms divide into 2 external wings (*E1* and *E2*). (F) Surface of a fully developed oral arm with many polygonal gaps (red) through which water and prey are transported. (G) Conic-shaped oral arm of a 3 mo old medusa (~3 cm bell diameter). (H) View of the oral arm canal system leading to the small mouth apertures, *M*; terminal appendages, *Ap*; small pore of the canal inlet, *P*; lateral canals leading to the apertures, *L*; main canal of the internal wing, *Mc*; central canal of the oral arm, *C*; digitata are not shown. Scale bars: (A–C) 0.5 mm, (D) 3 mm, (E,F) 1 mm, (G) 3 mm. Illustration: Silvia de Almeida Gonsales

currents, we quantified the mean (u_m) and maximum (u_{max}) swimming velocities and maximum velocities of feeding currents (u_f) produced by bell pulsations. Swimming (u_m, u_{max}) and feeding current velocities increased linearly with increases in bell diameter (Fig. 5B). Peak feeding current velocities, u_f, in small medusae (bell diameter <2 cm) were similar to peak swimming velocities, u_{max} (paired *t*-test, $t(4) = 1.84$, $p = 0.14$). However, in larger medusae, u_f became increasingly greater than u_{max}. The slope of the u_f linear regression was 1.29, while for u_m and u_{max} it was 0.35 and 0.61, respectively (Fig. 5B).

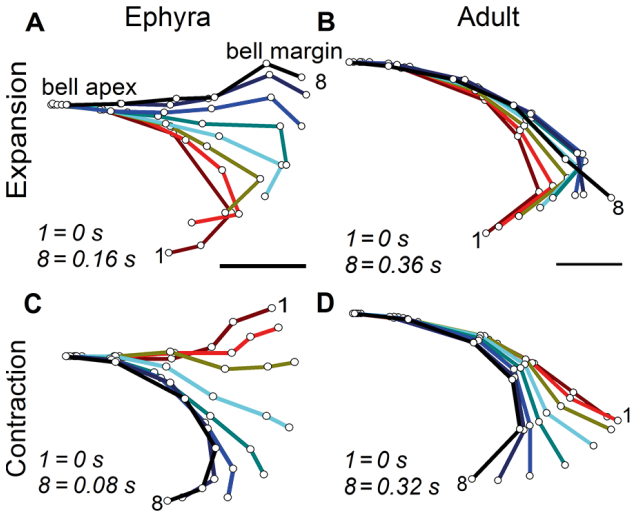

Fig. 3. Outlines of half of the bell of *Lychnorhiza lucerna* at equal time intervals (1–8), in (A,C) ephyra (scale = 1 mm), and (B,D) adult-shaped animal (scale = 10 mm), during (A,B) bell expansion and (C,D) contraction

Fluid transport to prey capture surfaces

Analysis of DPIV revealed the manner in which the flux of fluid generated during bell pulsations interacted with prey capture surfaces on oral arms. The DPIV revealed the formation of starting and stopping vortices during contraction and relaxation phases, respectively. At maximum contraction phase (Fig. 6, T = 0), the medusa was about to start bell expansion. The expansion of the bell resulted in the entrainment of fluids surrounding the exumbrella, with flow directed towards the subumbrella as a stopping vortex (Fig. 6, T = 50%). With maximum bell expansion (Fig. 6, T = 100%), fluid entrainment decreased and contraction was initiated (Fig. 6, lower panels). Between T = 0 and T = 50% (Fig. 6, lower panels), fluid surrounding the exumbrella circulated into a starting vortex. Maximum fluid velocities ($u_f \approx 9$ cm s^{-1}) were found near the bell margin at 50% contraction (t = 0.45 s). After the maximum contraction of the bell, water displacement kept adding energy to the rotation of the vortex (see Supplement 1 at www.int-res.com/articles/suppl/m557p145_supp/).

Fluid transport towards the prey capture surfaces were evaluated as the X axial velocity in cm s^{-1} (see 'Materials and methods') along transects on oral arms (Fig. 7). Fluid transport from the vicinities of the exumbrella towards the medusa's axis of symmetry (inside the bell and oral arms) are represented as negative values, whereas transport from the internal region to outside are positive values. In ephyrae, the highest velocities occurred immediately below the bell margin, at 25 and 50% of the period of total contraction. Velocities rapidly attenuated to between 75 and 100% of the contraction period. Because of this rapid dissipation, fluid velocities at the distal prey capture surfaces were nearly zero, or slightly positive. During bell expansion, fluid was also transported towards the animal's symmetry axis, but at slower velocities than during contraction. Fluid transport (as X axial velocities) produced during both bell contraction and expansion were less effective at producing fluid transport towards prey capture surfaces in ephyrae (Fig. 7A).

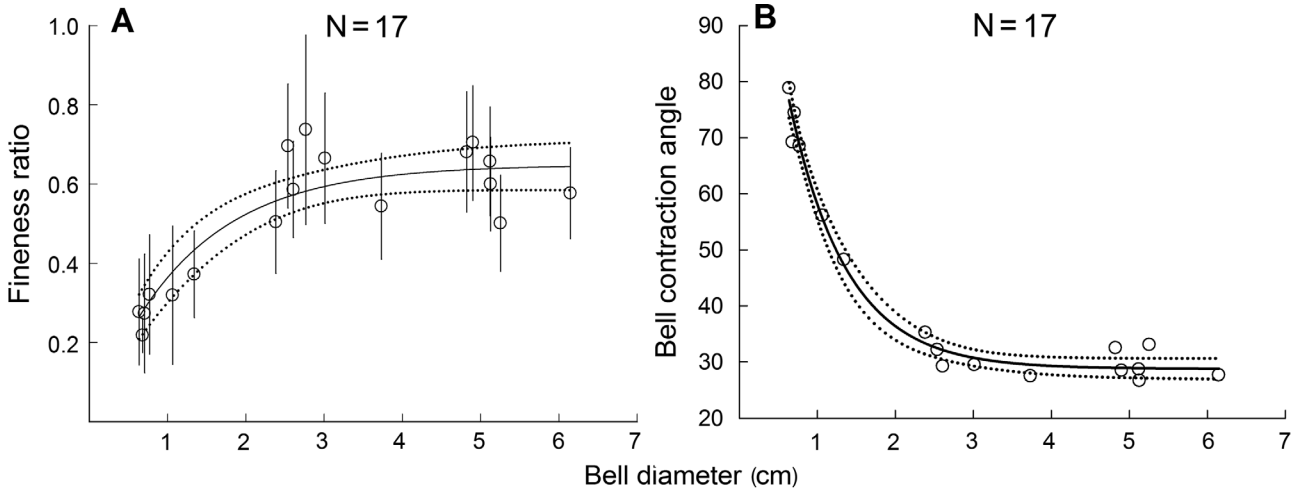

Fig. 4. Bell kinematics of *Lychnorhiza lucerna*. Changes in bell shape were quantified by (A) fineness ratio f and (B) bell contraction angle c, along the range of bell diameter (D, cm). Dotted lines: 95% CIs for the regressions. The regression lines shown (±95% CIs in parentheses) are: (A) $f = 0.65\ (\pm 0.03) \times \{1 - \exp[-0.82\ (\pm 0.13) \times D]\}$ ($r^2 = 0.81$, $p < 0.001$), and (B) $c = 28.77\ (\pm 0.87) + 113.03\ (\pm 11.80) \times \exp[-1.35\ (\pm 0.15) \times D]$ ($r^2 = 0.98$, $p < 0.001$)

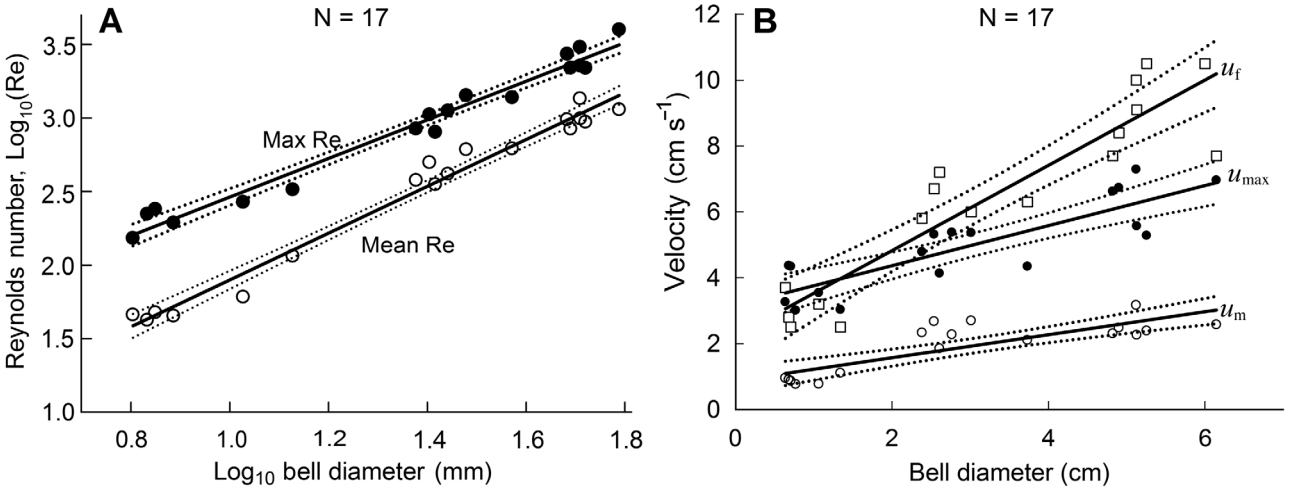

Fig. 5. (A) Relationship between body size, as bell diameter (D, mm) and $\log_{10}$ of mean and maximum Reynolds number (Re) in *Lychnorhiza lucerna*. (B) Relationships between bell diameter of *L. lucerna* and maximum swimming velocity (u_{max}), mean swimming velocity (u_m), and maximum velocity of feeding currents (u_f). Dotted lines: 95% CIs for the regressions. The regression lines shown (±95% CIs in parentheses) are as follows: (A) Log_{10}Max Re = 1.15 (±0.07) + 1.31 (±0.05) × Log_{10} D (r^2 = 0.97, $p < 0.0001$), and Log_{10}Mean Re = 0.31 (±0.08) + 1.59 (±0.05) × Log_{10} D (r^2 = 0.98, $p < 0.0001$); (B) u_{max} = 3.15 (±0.31) + 0.61 (±0.09) × D (r^2 = 0.73, $p < 0.0001$), and u_m = 0.87 (±0.20) + 0.35 (±0.05) × D (r^2 = 0.68, $p < 0.0001$), and u_f = 2.23 (±0.49) + 1.29 (±0.13) × D (r^2 = 0.85, $p < 0.0001$)

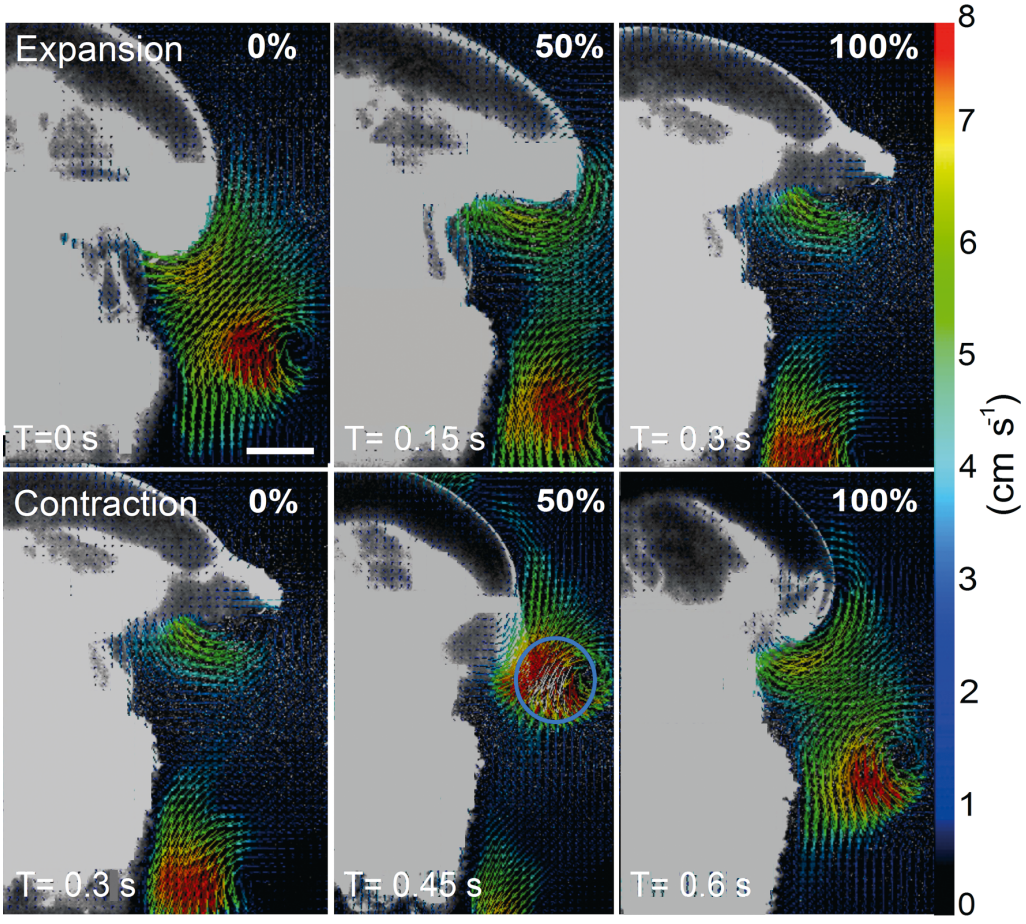

Fig. 6. Image sequence of the digital particle image velocimetry (DPIV) technique demonstrating the velocity of fluids (cm s^{-1}) surrounding a swimming medusa of *Lychnorhiza lucerna*. Upper panels show the expansion phase, when a stopping vortex is formed just below the bell margin, and surrounding fluids refill subumbrellar space. Lower panels demonstrate the contraction phase, when the starting vortex is formed and the highest velocities of the feeding currents (i.e. u_f) are shown at 50% (blue circle) of the period of bell contraction. The white vectors (inside the blue circle) at T = 0.45 s indicate velocities >8 cm s^{-1} (~9 cm s^{-1}). Scale bar = 1 cm

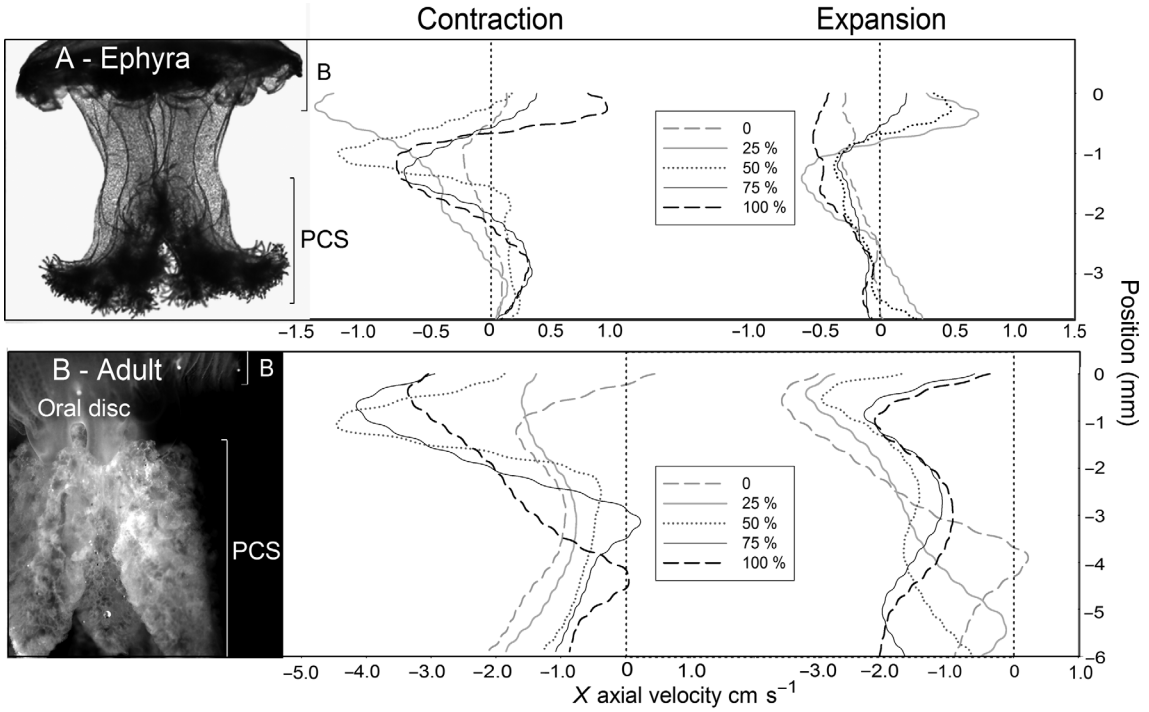

Fig. 7. Axial (*X*) velocities of fluids during both bell contraction and expansion of (A) an ephyra and (B) an adult-shaped medusa of *Lychnorhiza lucerna* of 4 and 26 mm bell diameter, respectively. Velocities were measured along a vertical transection from the umbrellar margin (position = 0 mm) to the end of the oral arm (position = –3.7 for the ephyra and –6 for the adult-shaped medusa). Each curve represents the instant velocities taken at 5 time intervals between the start (0) and the end (100%) of both movements. Fluid transport from the exumbrella towards the oral arms are represented as negative *X* axial velocities, whereas transport from the oral arms to the outside are positive *X* axial velocities. B = bell, PCS = prey capture surfaces

In adults (>26 mm), similarly to ephyrae, the transport of fluids towards the medusa's axis of symmetry occurred during both bell contraction and expansion, but peak velocities were found at between 50 and 100% of the total contraction period (Fig. 7B). The highest fluid transport velocities were found in the region of the oral disk, between the bell margin and the beginning of the prey capture surfaces (Fig. 7B). In contrast to ephyrae, starting vortices of adults did not immediately dissipate, but instead, moved distally away from the bell margin and continued to transport fluids towards prey capture surfaces. During both pulsation phases, a small velocity peak occurred at the end of oral arms of adults. This secondary peak, typically of a magnitude nearly half of the peak bell margin velocity, represented the remnants of starting vortices generated during the previous bell pulsation cycle, propagated away from the bell with continued transport of fluid and entrained particles towards the oral arm tips (Fig. 7B). At any one time, the most recent starting vortex as well as the remnant starting vortex from the previous bell contraction cycle traversed the length of adult oral arm exterior surfaces.

Although the DPIV technique provides high-resolution fluid velocity information, it permits limited insight into flows within the oral arm structures themselves. The fluorescein dye technique allowed the visualization of fluid transport from internal surfaces of oral arms through the prey capture structures. As the medusa expanded its bell, fluid was transported just below the bell margin to refill the subumbrellar cavity (Fig. 8A). During bell contraction, a starting vortex was formed and the border of the vortex ring encountered the oral arm (Fig. 8B). During the next bell expansion, and formation of its associated stopping vortex on the subumbrellar surface, the previous starting vortex rotated downstream along the exterior oral arm surfaces (Fig. 8C). As the next contraction began, the fluid previously transported to the inner region of the oral arms declined in velocity and diffused outward through the distal ends of oral arms (Fig. 8D,E).

The water entrained towards the subumbrellar surface traveled past the epidermal layer, which is covered by many motile cilia (Supplement 2). These cilia transported water distally toward the oral arms. The internal surfaces of the oral arms, including the digitata, are also covered by epidermal cilia which have movements of identical direction, but apparently in a non-synchronized beating pattern (Supplement 2).

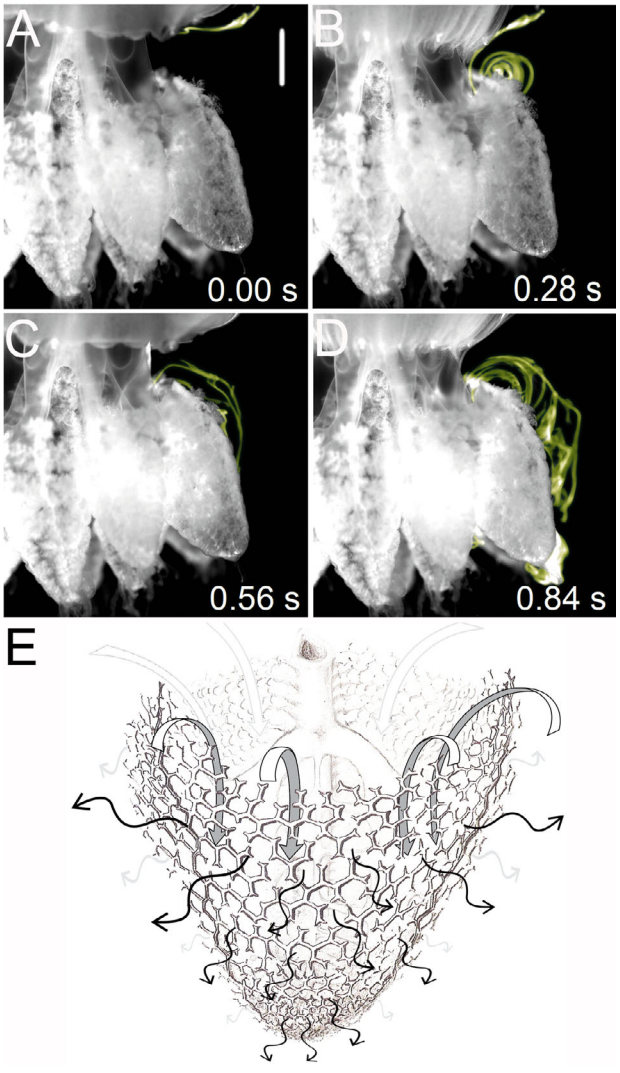

Fig. 8. Sequence of vortice formation during 2 bell pulsation cycles (A–D, T = 0.84 s) and interaction of vortex flows with oral arms of *Lychnorhiza lucerna*. (A) Fluorescein dye entrained within subumbrellar cavity, below bell margin at the first expansion. (B) Subsequent bell contraction and formation of a starting vortex, near the beginning of prey capture surfaces on the oral arms. (C) The next bell expansion and the previous starting vortex translating to inside the oral arms. (D) The next bell contraction and formation of the second starting vortex, while fluid entrained during the first pulsation cycle reaches the tip of the oral arm. (E) A schematic of the filtration mechanism of an oral arm. Scale bar = 1 cm. Illustration: Silvia de Almeida Gonsales

This ciliary beating generated currents that transport fluids from the interior spaces within the oral arms to the tips of digitata, where capture by nematocysts occurs. The digitata bear clusters of nematocysts (located on the digitata tips and bases) which retain prey before ingestion. The oral arm edges operate as filtering surfaces as vortices move along the edge surfaces. Simultaneously, fluid passes from regions inside the oral arms outwards (Fig. 8E) through the polygonal gaps formed during oral arm development (Fig. 2F).

Prey escape from medusan feeding currents

Prey responses to swimming *L. lucerna* medusae strongly influenced predator capture success. All encounters between *Acartia* spp. (N = 38) and *L. lucerna* medusae resulted in escape responses. However, 17% of encounters between *Temora turbinata* (N = 40) and *L. lucerna* medusae did not elicit evasive jumps by copepods, and those *T. turbinata* were then transported past the bell margin by medusan feeding currents toward the oral arms. Several sequences of copepod-medusa interactions are shown in Supplement 3. Table 1 summarizes copepod escape parameters during interactions with swimming *L. lucerna* medusae. For *Acartia* spp., escapes were primarily double jumps of short duration (~0.03 s), whereas for *T. turbinata*, escapes composed multiple jumps (~0.13 s), reaching greater total distances (~10.53 mm) (Table 1). The distance from a predator where copepods initiated escapes were higher for *Acartia* spp., which initiated escapes on average at ca. 5 body lengths (5.42 mm) from a predator, while *T. turbinata* often did not try to escape until drawn much closer to the predator (ca. 1 body length before the escape response, Table 1, Supplement 3). *Acartia* spp. escaped at angles wider than 90° (94% of the escapes) relative to the predator's feeding structures. In contrast, *T. turbinata* escape angles were more variable and escape angles narrower than 60° were frequently recorded (27%).

Depending on the location of where prey were transported, they became susceptible to capture by oral arms in different ways. When prey were transported to the interior of the oral arms, they were frequently confined in the spaces between oral arm wings. Prey then encountered digitata during navigation through the polygonal gaps in the oral arms (see Supplement 4). Prey were also vulnerable to capture when transported within starting vortex propagation along the exterior oral arm surfaces. Copepod escape angles were often inadequate for escape and resulted in their capture on oral arm surfaces (see Supplement 5).

Prey capture maps

In order to evaluate the relative importance of different regions of the oral arm structures for prey cap-

Table 1. Summary of escape response parameters of copepods to feeding currents generated by bell pulsations of *Lychnorhiza lucerna* (0.6–1.5 cm bell diameter). Means based on 38 escape reactions of *Acartia* spp. and 33 of *Temora turbinata*. Standard error and range are given in parentheses

Features of escape response	*T. turbinata*	*Acartia* spp.
Body length of copepod (mm)	0.99 (±0.19, 0.528–1.28)	1.12 (±0.24, 0.71–1.41)
Distance of reaction (mm)	1.26 (±1.27, 0–6.43)	5.42 (±3.06, 0–11.59)
Jump distance (mm)	10.53 (±5.07, 1.20–20.60)	2.92 (±1.51, 0.96–6.90
Max. velocity of jump (mm s^{-1})	182.3 (±61.27, 113.21–323.97)	203.28 (±124.11, 80.71–559.67)
Mean turn angle (°)	64.90 (±28.24, 8.21–172.13)	28.24 (±22.77, 0–103.34)
Escape angle relative to predator (°)	102.74(±50.06, 5.50–176.16)	140.68 (±25.93, 76.08–176.27)
Escape duration (s)	0.12 (±0.06, 0.03–0.28)	0.03 (±0.01, 0.01–0.6)

ture, we tabulated results of 5893 *Artemia* sp. nauplii that were captured on oral arms of 5 medusae. The absolute percentages of prey captures were significantly different between the different wings of the oral arms (ANOVA, $F_{2,12} = 5.59$, $p < 0.05$), with higher captures on external wing 2 in relation to the internal wing (Tukey's test, $p < 0.05$) (Fig. 9). There were no significant differences between regions (1–6) along the internal wing of the oral arm (ANOVA, $F_{5,24} = 2.34$, $p = 0.07$). However, regions along the length of external wing 1 (ANOVA, $F_{4,20} = 8.07$, $p < 0.001$) and external wing 2 (ANOVA, $F_{4,20} = 10.73$, $p < 0.001$) did exhibit significantly more captures along regions 3 and 4 than region 6 for external wing 1, and lower captures at region 6 than any other region, for the external wing 2 (Tukey's test, $p < 0.05$). Differences in the absolute number of captures on different oral arm wings were related to differences in areas of the oral arm wings because, when normalized by the area available for capture, there were no significant differences in capture rates between the 3 wings (Kruskal-Wallis, $\chi^2(2) = 5.79$, $p = 0.06$).

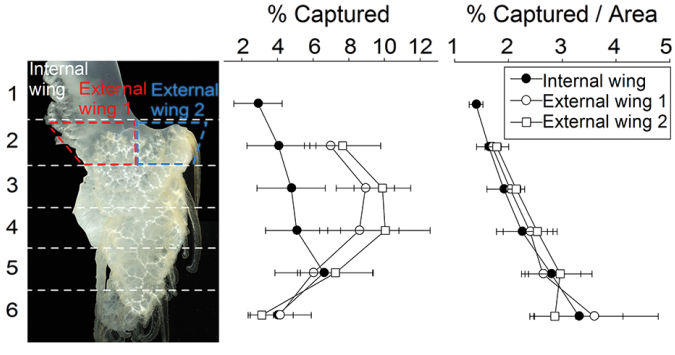

Fig. 9. Prey captures (mean ± SD) along oral arms of *Lychnorhiza lucerna* (N = 5). The 3 oral wings were divided into regions (1–6 for the internal wing or 2–6 for the external wings) in relation to the distance from the bell. Only region 1 of the internal wing is shown

DISCUSSION

Morphological transition and development of filtering oral arms

Similarly to other members of the Rhizostomeae, *Lychnorhiza lucerna* undergoes a series of morphological changes in its feeding apparatus during early development (Uchida 1926, Sugiura 1966, Holst et al. 2007, the present study). Scyphozoan ephyrae lack specialized feeding structures (e.g. tentacles and oral arms), and capture prey along the subumbrellar surface and marginal lappets (Sullivan et al. 1997, Higgins et al. 2008). Recently released *L. lucerna* ephyrae rapidly develop digitata along mouth edges (Fig. 2B), which are the first specialized capture structures. In the viscous fluid environment of ephyrae ($Re < 10^2$), momentum transfer of flow is minimal and bell pulsations are less effective in producing flows through the digitata (Fig. 7A). As medusae grow, inertial forces become increasingly dominant and bell pulsations become effective for pumping fluid along the oral arm surfaces. Adult medusae develop structures within the oral arms that contain numerous filtration gaps (Fig. 2F). This developmental transition occurs during a shift in hydrodynamic regime that includes higher Re flows and more fully developed vortex generation at the bell margin. The larger vortices strongly influence prey transport and the locations of prey capture. These transitions in morphology and feeding mechanics determine a biomechanical framework within which predation by rhizostome ephyrae and young medusae occurs.

Changes in bell shape during early development in *L. lucerna* affected both bell pulsation patterns and the propulsion mode. The change of an oblate ephyral bell (fineness ratio $f = 0.2–0.4$) into a prolate bell ($f = 0.5–0.8$) reduces drag by streamlining, which increases swimming efficiency in an inertially domi-

nated fluid environment (Re < 10^3) (Colin et al. 2013). In ephyrae, the longer stroke lengths of bell pulsation (Figs. 3 & 4B) are characteristic of drag-based paddling (Blough et al. 2011), which is a common strategy for animals living in lower Re (Vogel 2003, Higgins et al. 2008, Feitl et al. 2009). In this propulsive mode, forward thrust ceases after the power stroke and the wider strokes enable higher thrust production, since forward thrust is directly related to stroke length (Vogel 2003, Blough et al. 2011). In contrast, swimming by adults involves movements primarily by the bell margin. These adult bell pulsations produce 2 opposite rotational vortices, which generate forward thrust and transport prey to prey capture structures (Dabiri et al. 2005). These results demonstrate that the transition in fluid environments accompanying development was accompanied by alterations in both propulsive and feeding strategies of *L. lucerna*.

Fluid transport to prey capture surfaces

Swimming (u_m and u_{max}) velocities increased with medusa size. However, feeding current velocities (u_f) increased more rapidly with bell size than did swimming velocities. Higher feeding current velocities are important for the dietary niche because they allow the transport of more evasive prey (Costello & Colin 1994). Maximum u_f were found at the interface between stopping and starting vortices, at ~50% of bell contraction (Fig. 6). Dabiri et al. (2005) argued that momentum flux increased at the interfaces of these vortices. These vortex interactions increase u_f, which enhances fluid transport as well as entrainment of more evasive prey.

Although the production of feeding currents via bell pulsations is widely used among large medusae (Costello & Colin 1995), the shape and positioning of feeding structures in relation to swimming vortices vary between medusan species. This may result in distinct modes of prey capture and prey selectivity. In medusae with marginal tentacles, like the scyphozoan *Aurelia* sp. and the hydrozoan *Aequorea victoria*, tentacles lie in the center of the starting vortex (Dabiri et al. 2005, Lipinski & Mohseni 2009). Nevertheless, rhizostome medusae lack marginal tentacles and have a great diversity of bell morphologies and oral arm shapes, which may generate distinct modes of interactions between vortices of bell pulsation and oral arms (Fig. 6). In *L. lucerna*, only the edge of the vortex contacts oral arms, while the center of the vortex moves freely downwards, outside the oral arm surface, and entrains surrounding fluids towards the oral arms. This pattern is different from that of the rhizostome *Cassiopea* sp., which has a flatter bell and oral arms that extend far from the animal's symmetry axis. The entire vortex (not only its inside edge) translates through the oral arms of *Cassiopea* sp. (Hamlet et al. 2011, Santhanakrishnan et al. 2012).

Velocity fields determined by DPIV demonstrated that vortices transported fluids to the oral arms, where particles were retained. For *L. lucerna*, a division of the entrained fluids occurs so that only a small portion of the starting vortex is channeled to the inner oral arms (Figs. 6–8), whereas the majority of the starting vortex travels downstream along the exterior of the oral arms. This downstream propagation of the starting vortex enables fluid transport along the external wings of the oral arms (Fig. 7B), and transport of prey to the external oral arm wings (Fig. 9), where they are captured by digitata lining the exterior oral arm wings.

Unlike the fluid that flows along the exterior oral arm surfaces, the fluid that is transported into the inner oral arms (Fig. 6) becomes confined within the cavities formed by the 3 wings of the oral arms. This water is then pushed from the interior of the oral arms through the filtering gaps to the oral arm exterior by ciliary currents generated along the epidermal surfaces of the highly complex (Fig. 2G,H) oral arm body. Due to the size of these gaps (Fig. 2E,F), smaller particles can pass freely to the outside. However, larger particles are trapped and retained by nematocysts lining the digitata. The similarity of digitata dimensions among rhizostome medusae (Fig. 10) suggests that patterns found for *L. lucerna* may be more widely applicable to other rhizostome medusae.

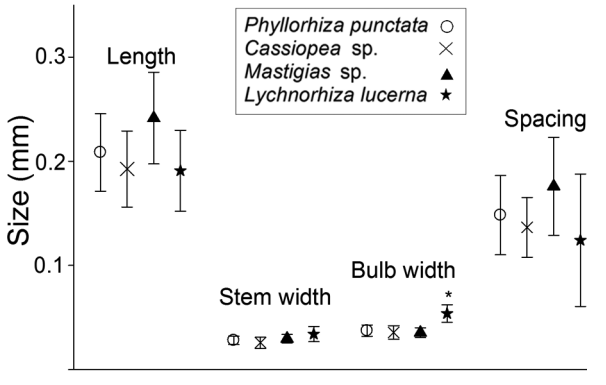

Fig. 10. Morphological features of digitata in medusae of Rhizostomeae. A total of 778 measurements were taken of 3–4 individuals per species (~55 measurements per individual). Among these parameters, only the bulb width of digitata of *Lychnorhiza lucerna* were significantly larger than other species (ANOVA-NESTED, $F_{3,9}$ = 23.61, *p < 0.0001)

Prey escape from medusan feeding currents

Calanoid copepods possess well-developed escape responses to predators (Burdick et al. 2007, Buskey et al. 2012) and might be expected to elude the comparatively slow-feeding current velocities of *L. lucerna.* The copepods *Acartia* spp. and *Temora turbinata* are the dominant co-occurring mesozooplankton with *L. lucerna* (Nagata & Morandini unpubl.) and are capable of escape swimming velocities between 10 and 55 cm s^{-1} (Table 1). These escape velocities are up to 5× faster than maximum velocities of *L. lucerna*'s feeding currents (u_f < 10 cm s^{-1}; Fig. 5B). Although the robust pulsations of rhizostome medusae produce comparatively rapid feeding currents relative to other scyphozoans (e.g. *Aurelia* sp.: <3 cm s^{-1}, and *Chrysaora quinquecirrha*: ~5 cm s^{-1} for individuals <8 cm of bell diameter; D'Ambra et al. 2001, Santhanakrishnan et al. 2012, respectively), these feeding current velocities may still be insufficient to exceed escape velocities of co-occurring copepods. The few field data on rhizostome feeding habits provide equivocal evidence that calanoids may both avoid predation (Larson 1991, Álvarez-Tello et al. 2016), or be captured in similar proportions to environmental densities (Fancett 1988, Nagata 2015).

On the other hand, it is important to emphasize that prey items of limited escape ability may also avoid predation by failing to elicit a retention response on a predator's capture structures. Several sequences (Supplement 6 at www.int-res.com/articles/suppl/m557p145_supp/) demonstrated the absence of capture reactions by the digitata, especially in the case of contact with diatoms (*Coscinodiscus* sp.). Further studies are needed to better characterize the details of post-encounter between medusae and their prey, since retention efficiency is among the main parameters governing prey capture success (Riisgård 1988, Jaspers et al. 2011).

How do these medusae succeed at capturing copepods despite the capability of copepods to simply swim out of a medusa's feeding current? Actually, most encounters between *L. lucerna* and copepods that we observed resulted in escape by the copepod and indicated low capture efficiencies by the medusae on calanoid copepods. However, we also found circumstances that favored successful capture of copepods by medusae. During some predator-prey encounters, copepod prey failed to detect the medusan predator's feeding current and no escape response occurred prior to contact between predator and prey. In 17% of encounters, *T. turbinata* did not react within flows created by *L. lucerna* and were subsequently transported by predator feeding currents. In contrast, *Acartia* spp. were more reactive and initiated evasive jumps at distances about 5× greater from *L. lucerna* than did *T. turbinata* (Table 1). Such a difference in reactivity between species is consistent with recorded shear threshold sensitivities, for which *Acartia* spp. appears to respond to shear deformations about 5× smaller than *Temora* sp. (Colin et al. 2010). *Acartia* spp. generally avoided medusae by escaping feeding currents before reaching a medusa's bell margin, whereas *T. turbinata* allowed transport within medusan feeding currents and sometimes appeared not to detect an approaching medusa. A second potential source of copepod capture was observed to occur after a copepod appeared to detect the feeding current of a medusa but subsequently made a high-speed escape jump into, rather than away from, the medusa. Such 'wrong direction' escape movements can occur because, as documented with artificial hydrodynamic disturbances (e.g. Buskey et al. 2002), copepods do not always reorient with reference to a hydrodynamic cue prior to escape jumping. The high amount of vorticity within medusan feeding currents may further obscure the hydrodynamic directionality that is most favorable for a copepod escape jump. *Acartia* spp. performed escape jumps primarily in the opposite direction of medusan feeding current flows and thereby avoided entrainment within feeding currents. On the other hand, the narrower escape jump angles (<60°) in 27% of the encounters with *T. turbinata* made them vulnerable to feeding current transport toward the oral arms (Figs. 6 & 7). Escape jumps by *T. turbinata* sometimes inadvertently led the prey towards the oral arms and resulted in capture (Supplement 5). Thus, due to mismatches in detection thresholds or escape directions, medusae may capture rapidly swimming prey despite the disparities between medusan feeding current and prey escape velocities. Thus, our starting hypothesis that calanoid copepods would be sensitive to hydrodynamic disturbances created by medusae and subsequently escape requires qualification. *Acartia* spp. did generally escape and *T. turbinata* often escaped. However, failure to detect the medusan predator and mis-directed escape efforts resulted in copepod captures by *L. lucerna*. The frequency with which these interactions occur in nature influences the ability of these medusae to exploit a wide range of available prey within plankton communities.

Acknowledgements. This study was partially funded by grants 1536672 and 1536688 from the National Science Foundation's Division of Ocean Science (NSF/OCE), 2010/50174-7, 2011/00436-8, 2011/50242-5, 2013/19478-8, 2014/00824-6, 2015/01307-8 and 2016/05637-5 from the São Paulo Research Foundation (FAPESP), grant 301039/2013-5 from the Conselho Nacional de Desenvolvimento Científico e Tecnológico (CNPq), and support from Programa de Excelência Acadêmica da Coordenação de Aperfeiçoamento de Pessoal de Nível Superior (CAPES PROEX). The study is a contribution of Núcleo de Pesquisa em Biodiversidade Marinha da Universidade de São Paulo (NPBioMar, USP). We thank the Oceanographic Institute of the University of São Paulo (IO-USP) and Centro de Biologia Marinha (CEBIMar-USP) for providing facilities at the coast. We thank the staff of Projeto Garoupas (FAPESP 2011/50407-4) for allowing the use of tanks for cultivating our jellyfish. We also thank Nilvea Ramalho de Oliveira, Leandro Santos, and Elso Alves da Silva for their valuable support in cultivating the experimental animals.

LITERATURE CITED

Acuña JL, López-Urrutia A, Colin S (2011) Faking giants: the evolution of high prey clearance rates in jellyfishes. Science 333:1627–1629

Álvarez-Tello F, López-Martinez J, Lluch-Cota DB (2016) Trophic spectrum and feeding pattern of cannonball jellyfish *Stomolophus meleagris* (Agassiz, 1862) from central Gulf of California. J Mar Biol Assoc UK 96:1217–1227

Blough T, Colin SP, Costello JH, Marques AC (2011) Ontogenetic changes in the bell morphology and kinematics and swimming behavior of rowing medusae: the special case of the limnomedusa *Liriope tetraphylla.* Biol Bull (Woods Hole) 220:6–14

Burdick DS, Hartline DK, Lenz PH (2007) Escape strategies in co-occurring calanoid copepods. Limnol Oceanogr 52: 2373–2385

Buskey EJ, Lenz PH, Hartline DK (2002) Escape behavior of planktonic copepods in response to hydrodynamic disturbances: high speed video analysis. Mar Ecol Prog Ser 235:135–146

Buskey EJ, Lenz PH, Hartline DK (2012) Sensory perception, neurobiology, and behavioral adaptations for predator avoidance in planktonic copepods. Adapt Behav 20:57–66

Colin SP, Costello JH, Hansson LJ, Titelman J, Dabiri JO (2010) Stealth predation and the predatory success of the invasive ctenophore *Mnemiopsis leidyi.* Proc Natl Acad Sci USA 107:17223–17227

Colin SP, Costello JH, Katija K, Seymour J, Kiefer K (2013) Propulsion in cubomedusae: mechanisms and utility. PLOS ONE 8:e56393

Costello JH, Colin SP (1994) Morphology, fluid motion and predation by the scyphomedusa *Aurelia aurita.* Mar Biol 121:327–334

Costello JH, Colin SP (1995) Flow and feeding by swimming scyphomedusae. Mar Biol 124:399–406

Costello JH, Colin SP, Dabiri JO (2008) Medusan morphospace: phylogenetic constraints, biomechanical solutions, and ecological consequences. Invertebr Biol 127: 265–290

Dabiri JO, Colin SP, Costello JH, Gharib M (2005) Flow patterns generated by oblate medusan jellyfish: field measurements and laboratory analyses. J Exp Biol 208: 1257–1265

D'Ambra I, Costello JH, Bentivegna F (2001) Flow and prey capture by the scyphomedusa *Phyllorhiza punctata* von Lendenfeld 1884. Hydrobiologia 451:223–227

Fancett MS (1988) Diet and selectivity of scyphomedusae from Port Phillip Bay, Australia. Mar Biol 98:503–509

Feitl KE, Millett AF, Colin SP, Dabiri JO, Costello JH (2009) Functional morphology and fluid interactions during early development of the scyphomedusa *Aurelia aurita.* Biol Bull (Woods Hole) 217:283–291

Fossette S, Gleiss AC, Chalumeau J, Bastian T and others (2015) Current-oriented swimming by jellyfish and its role in bloom maintenance. Curr Biol 25:342–347

Hamlet C, Santhanakrishnan A, Miller LA (2011) A numerical study of the effects of bell pulsation dynamics and oral arms on the exchange currents generated by the upside-down jellyfish *Cassiopea xamachana.* J Exp Biol 214:1911–1921

Hays GC, Bastian T, Doyle TK, Fossette S and others (2012) High activity and Lévy searches: jellyfish can search the water column like fish. Proc R Soc B 279:465–473

Higgins JE, Ford MD, Costello JH (2008) Transitions in morphology, nematocyst distribution, fluid motions, and prey capture during development of the scyphomedusa *Cyanea capillata.* Biol Bull (Woods Hole) 214:29–41

Holst S, Sotje I, Tiemann H (2007) Life cycle of the rhizostome jellyfish *Rhizostoma octopus* (L.) (Scyphozoa, Rhizostomeae), with studies on cnidocysts and statoliths. Mar Biol 151:1695–1710

Jarms G, Morandini AC, Silveira FL (2002) Cultivation of polyps and medusae of Coronatae (Cnidaria, Scyphozoa) with a brief review of important characters. Helgol Mar Res 56:203–210

Jaspers C, Titelman J, Hansson LJ, Haraldsson M, Ditlefsen CR (2011) The invasive ctenophore *Mnemiopsis leidyi* poses no direct threat to Baltic cod eggs and larvae. Limnol Oceanogr 56:431–439

Kawahara M, Uye S, Ohtsu K, Iizumi H (2006) Unusual population explosion of the giant jellyfish *Nemopilema nomurai* (Scyphozoa: Rhizostomeae) in East Asian waters. Mar Ecol Prog Ser 307:161–173

Koehl MAR (2004) Biomechanics of microscopic appendages: functional shifts caused by changes in speed. J Biomech 37:789–795

Koehl MAR, Koseff JR, Crimaldi JP, McCay MG, Cooper T, Wiley MB, Moore PA (2001) Lobster sniffing: antennule design and hydrodynamic filtering of information in an odor plume. Science 294:1948–1951

Kramp PL (1970) Zoogeographical studies on Rhizostomeae (Scyphozoa). Vidensk Meddr Dansk Naturh Foren 133: 7–30

Larson RJ (1991) Diet, prey selection and daily ration of *Stomolophus meleagris*, a filter-feeding scyphomedusa from the NE Gulf of Mexico. Estuar Coast Shelf Sci 32: 511–525

Lipinski D, Mohseni K (2009) Flow structures and fluid transport for the hydromedusae *Sarsia tubulosa* and *Aequorea victoria.* J Exp Biol 212:2436–2447

Morandini AC (2003) Estrutura populacional de *Chrysaora lactea* e *Lychnorhiza lucerna* (Cnidaria; Scyphozoa) em amostras de plâncton, com a redescrição das espécies. PhD dissertation, Universidade de São Paulo

Nagata RM (2015) Bases morfo-funcionais da alimentação e o papel trófico de *Lychnorhiza lucerna* (Scyphozoa, Rhizostomeae). PhD dissertation, Instituto de Biociências da Universidade de São Paulo

Nagata RM, Haddad MA, Nogueira M Jr (2009) The nuisance of medusae (Cnidaria, Medusozoa) to shrimp trawls in central part of southern Brazilian Bight, from the perspective of artisanal fishermen. Pan-Am J Aquat Sci 4:312–325

Nogueira M Jr (2006) Macrozooplâncton gelatinoso do litoral do Paraná: composição, abundância e aspectos ecológicos. Masters dissertation, Universidade Federal do Paraná

Raskoff KA, Sommer FA, Hamner WM, Cross KM (2003) Collection and culture techniques for gelatinous zooplankton. Biol Bull (Woods Hole) 204:68–80

Riisgård HU (1988) Efficiency of particle retention and filtration rate in 6 species of northeast American bivalves. Mar Ecol Prog Ser 45:217–223

Russell FS (1970) The medusae of the British Isles, Vol II: pelagic Scyphozoa. Cambridge University Press, Cambridge

Santhanakrishnan A, Dollinger M, Hamlet CL, Colin SP, Miller LA (2012) Flow structure and transport characteristics of feeding and exchange currents generated by upside-down *Cassiopea* jellyfish. J Exp Biol 215: 2369–2381

Schiariti A, Kawahara M, Uye SI, Mianzan HW (2008) Life cycle of the jellyfish *Lychnorhiza lucerna* (Scyphozoa: Rhizostomeae). Mar Biol 156:1–12

Sugiura Y (1966) On the life-history of rhizostome medusae. IV. *Cephea cephea.* Embryologia (Nagoya) 9: 105–122

Sullivan BK, Suchman C, Costello JH (1997) Mechanisms of prey selection by ephyrae of the scyphomedusa *Aurelia aurita.* Mar Biol 130:213–222

Uchida T (1926) The anatomy and development of a rhizostome medusa, *Mastigias papua* L. Agassiz, with observations on the phylogeny of Rhizostomae. J Fac Sci Tokyo Univ (Sect 4, Zool) 1:45–95

Vogel S (2003) Comparative biomechanics: life's physical world. Princeton University Press, Princeton, NJ

Editorial responsibility: Robert Condon, Wilmington, North Carolina, USA

Submitted: December 28, 2015; Accepted: August 1, 2016
Proofs received from author(s): September 15, 2016